ELSEVIER

PII: S0032-3861(96)00829-4

Polymer Vol. 38 No. 11, pp. 2797–2805, 1997

0032-3861/97/$17.00 + 0.00

Characterization of stress-whitening of tensile yielded isotactic polypropylene

Yan Liu
Department of Mining, Minerals and Materials Engineering, The University of Queensland, St. Lucia, Queensland 4072, Australia

and Colin H. L. Kennard and Rowan W. Truss*
Department of Chemistry, The University of Queensland, St. Lucia, Queensland 4072, Australia

and Nicholas J. Calos
Centre for Electron Microscopy and Microanalysis, The University of Queensland, St. Lucia, Queensland 4072, Australia
(Received 6 September 1995; revised 24 June 1996)

The microstructure of tensile tested isotactic polypropylene (iPP) specimens was studied by grey level measurement, scanning electron microscopy (SEM), differential scanning calorimetry (d.s.c.) and X-ray diffraction (XRD). SEM revealed that the necked regions of specimens in which stress-whitening had occurred as determined by the grey level measurement had craze-like structures which were parallel to the drawing direction. D.s.c. analysis showed that the necked regions of tensile specimens which remained transparent after yielding had an additional low-melting temperature peak. However, no additional melting peaks were found in the stress-whitened specimens. Inspection of the XRD patterns indicated that, apart from its original α-crystallites (a monoclinic structure) which were broken and reoriented after drawing, there was no new types of crystals formed in the transparent specimens. It was found by quantitative XRD analysis that the crystallites were broken into finer pieces in the whitened specimens than in the transparent ones. © 1997 Elsevier Science Ltd.

(Keywords: iPP; stress-whitening; SEM)

INTRODUCTION

The yielding behaviour of polymer materials has been studied for years[1–4] because it is an important property of these materials in load bearing application and also because it is still not well understood. For a viscoelastic polymer, the yielding point can be considered to be associated with the onset of significant plastic flow[5,6]. On a molecular level, the yielding is associated with inter-chain sliding, chain segmental motion and chain reconformation, which are characterized as rate processes[7]. The yielding behaviour of such polymer materials is thus sensitive to changes in temperature, strain rate and pressure[8–10]. Under tension, the spherulitic texture which frequently forms in a semicrystalline polymer is deformed. Upon yielding the spherulitic structure is destroyed and transformed into a fibrillar structure[11,12]. Additionally, during yielding crazing and stress-whitening may occur[13–15].

In our earlier work, the occurrence of crazing and stress-whitening in polypropylene (iPP) was found to be dependent on temperature and strain rate[16]. Furthermore in differential scanning calorimetry (d.s.c.) study, stress-whitened specimens showed only one melting peak, while those that remained transparent had two melting peaks[16] but the origin of the addition peak was unknown[16,17]. Examination by SEM revealed that micro-voiding occurred in the whitened specimens[16].

It has been found in small angle X-ray scattering (SAXS) studies[1,18] that, in the necked region of iPP drawn at high temperature, there are large numbers of densely packed and preferentially oriented continuous chains. The yielding conditions of these studies would produce transparent specimens according to the results of our study[16,19]. However, the arrangement of molecular chains in the whitened specimens and the correlation between the micellar structure and stress-whitening are still unclear.

Many theories and models have been proposed to describe the yielding process of viscoelastic polymers[6,20–23]. Among these theories, Eyring's viscosity theory has proved highly applicable. This theory models the yielding of polymers as a thermally activated rate process[24–27]. Frequently, two such processes, Process I and Process II, are required in order to adequately describe the yielding behaviour over a wide range of temperatures and strain rates[28–33]. In our previous study of the yielding of isotactic polypropylene (iPP)[16], it was found that the yield stress over temperature vs strain rate diagram could be divided into two regions: Region α

* To whom correspondence should be addressed

where Process I predominated and Region β where Process II was activated. Moreover, it was found by grey level measurements[16] that stress-whitening occurred in the necked regions of those tensile specimens which yielded under conditions of Region β.

In this paper, further results concerning the stress-whitening of iPP occurring in tensile yielding are presented. X-ray diffraction (XRD) was used to investigate the change in the crystal orientation and the arrangement of molecular chains in the specimens after yielding and also to reveal whether any new crystal structures had formed. The procedure for d.s.c. analysis was refined to suppress the influence of thermal contraction of the specimen on testing resulting in improved reproducibility of the test results. The deformed specimen was further characterized by grey level measurements and SEM. The results showed consistency with the previously reported results which allowed correlations between the stress-whitening, micro-voiding, d.s.c. and XRD results to be made.

EXPERIMENTAL

Specimens and tensile testing

The iPP used was a general purpose moulding grade homopolymer, 'Propathene' GXM43, in the form of extruded pellets supplied by ICI Australia, Plastics Group. These pellets were hot pressed between two stainless plates at 220°C and quenched in water to room temperature to form sheets of about 0.5 mm thick[34]. Dumbbell shaped specimens which had a gauge length of 10 mm and a width of 2.8 mm were cut from these sheets and tensile tested at temperatures of 21, 25, 40 and 56°C with strain rates of 8.33×10^{-3}, 8.33×10^{-2} and 8.33×10^{-1} s^{-1}. All the specimens were drawn approximately to a strain of 250%.

SEM

The specimens were fractured parallel to the loading direction after cooling in liquid nitrogen for 30 min and the fractured surfaces of the specimens were then carbon coated for investigation by SEM with a Jeol 6400 instrument operating at 5 kV.

D.s.c.

The thermal properties of the deformed specimens were analysed by a d.s.c. instrument, Perkin Elmer DSC7. The heating rate used was 20°C min^{-1}. Each specimen weighed about 3 mg. For comparison, specimens cut from original iPP sheets were also examined. All the data were later normalized to specimen weight of 1 mg.

Because the specimens for d.s.c. analysis were drawn, they contracted significantly upon melting which changed the thermal contact between the specimen and sample pan and consequently may have affected the reliability of the measurement[17]. To counteract this contraction, a restrained method has been reported[35]. However, this method may induce additional stress in the specimen and may also damage the microstructure of interest in the drawn polymer. In the present work, a new method was developed for improving the thermal contact between the specimen and sample pan. With this method, the specimen was immersed in a drop of diffusion pump (DP) fluid (about 14 mg) in the sample pan. The DP fluid used was SANTOVAC which had a boiling temperature of 295°C under vacuum. It was considered that the DP fluid could provide a reliable thermal contact between the specimen and sample pan that would not be affected by the contraction of the specimen upon melting. The d.s.c. curve of the DP fluid was a straight inclined line in the temperature range of interest to this study, i.e. 30–200°C. The curve from the DP fluid was later used for baseline subtraction in the drawn iPP d.s.c. analysis. No chemical reaction was found between the DP fluid and iPP specimens, and consistent results that had not been affected by melting contraction of the specimens were obtained.

XRD

The XRD patterns were obtained with a Philips PW1010 X-ray generator using Ni-filtered Cu$K\alpha$ radiation (40 kV, 20 mA) equipped with a Weissenberg camera. The drawn specimen was clamped in a goniometer head. Oscillation photographs (10°) were taken. The exposure time was about 30 min. For quantitative analysis, the XRD data from tensile tested iPP were collected from 2°C to 37° 2θ in 0.1° steps using graphite monochromated Cu$K\alpha$ radiation with a Siemens D5000 diffractometer. The regions not of interest were masked with Pb tape during data collection. The XRD data were analysed using the Rietveld profile-fitting package, SIROQUANT[36]. In this profile-fitting, the intrinsic profile of the diffractometer was standardized using diamond powder. The XRD trace was modelled with the structure of α-iPP determined by Mencik[37], i.e. a monoclinic lattice of $a = 6.63$ Å, $b = 20.78$ Å, $c = 6.504$ Å, $\alpha = \gamma = 90°$ and $\beta = 99.5°$ and space group $P2_1/c$. Furthermore, a bimodal particle size distribution[38] was used to fit the two components system of both amorphous and crystalline iPP.

The (0 0 2) texture pattern of iPP tested at 21°C and 8.33×10^{-1} s^{-1} was collected using graphite monochromated Mo$K\alpha$ radiation, with an ENRAF-NONIAS CAD4 K diffractometer.

RESULTS AND DISCUSSION

Stress-whitening characterization

Table 1 shows the tensile testing conditions and the occurrence of stress-whitening as characterized by grey level measurement[16] for the iPP specimens which were used in subsequent experiments. The whitened specimens are marked with 'Yes' while the transparent ones are indicated by 'No'. The specimens tested at 21°C were very white, while those yielded at 40 and 56°C were transparent. The specimens yielded at 25°C were slightly whitened and the whiteness increased with strain rate. Analysis of the test conditions showed that the specimens

Table 1 Results of stress-whitening characterization of the necked region of iPP tensile specimens tested at different conditions

Temperature (°C)	Strain rate (s^{-1})		
	8.33×10^{-3}	8.33×10^{-2}	8.33×10^{-1}
21	Yes	Yes	Yes
25	No	Yes	Yes
40	No	No	No
56	No	No	No

Yes = whitened; No = transparent

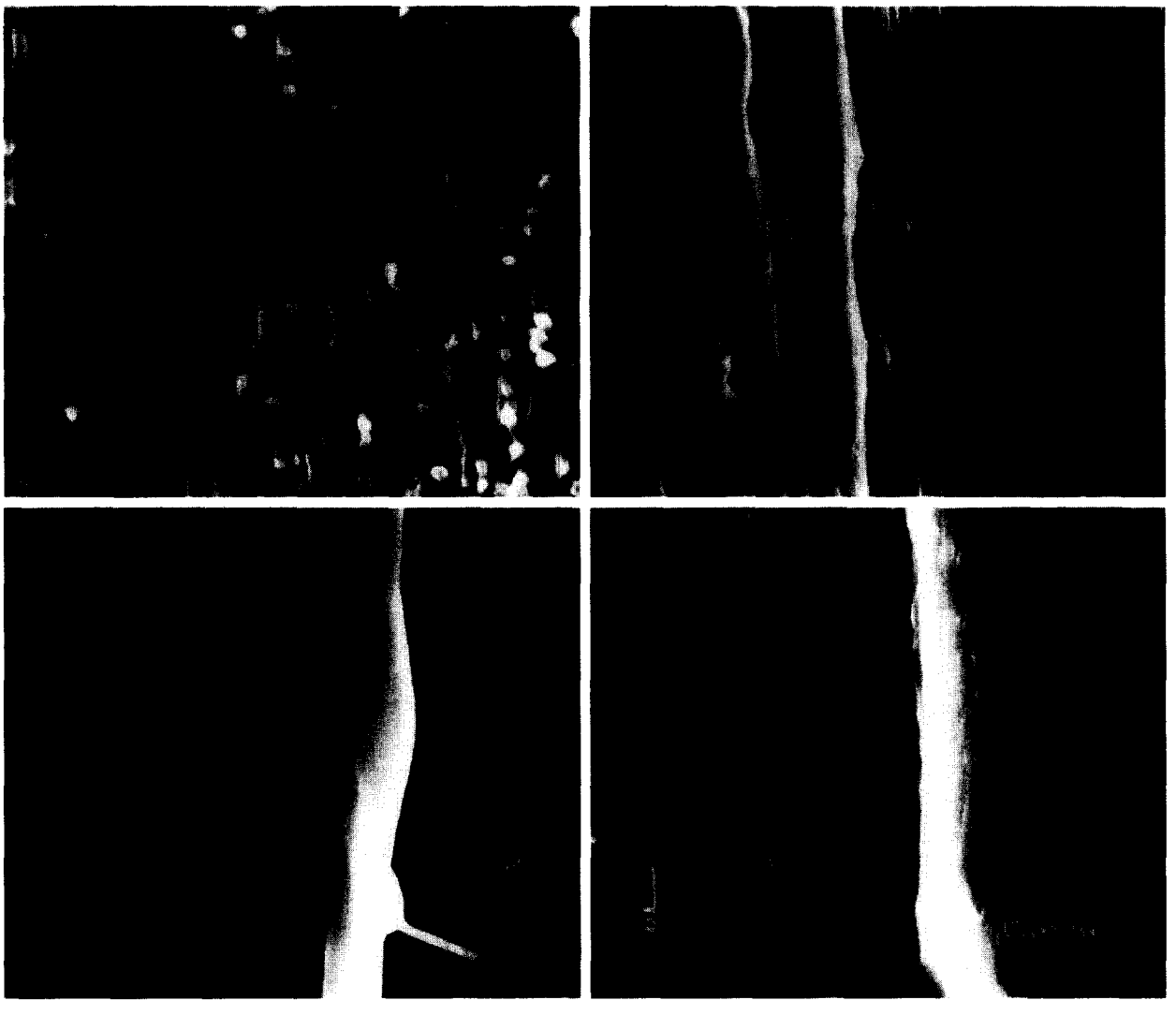

Figure 1 SEM micrographs showing typical morphologies of the longitudinally fractured surfaces of tensile yielded iPP specimens tested respectively at: (a) 21°C and $8.33 \times 10^{-3}\ s^{-1}$; (b) 21°C and $8.33 \times 10^{-1}\ s^{-1}$; (c) 56°C and $8.33 \times 10^{-3}\ s^{-1}$; and (d) 56°C and $8.33 \times 10^{-1}\ s^{-1}$

yielded at 40 and 56°C fell into Region α and those yielded at 21°C into Region β[16]. Those tested at 25°C were near the α to β transition boundary[16]. Thus the results presented in *Table 1* were consistent with the previous finding that stress-whitening was associated with the Process II activated yielding[16].

SEM investigation

Figure 1 shows SEM micrographs of the longitudinally fractured surfaces of four tensile specimens tested respectively at a temperature and strain rate of: (a) 21°C and $8.33 \times 10^{-3}\ s^{-1}$; (b) 21°C and $8.33 \times 10^{-1}\ s^{-1}$; (c) 56°C and $8.33 \times 10^{-3}\ s^{-1}$; and (d) 56°C and $8.33 \times 10^{-1}\ s^{-1}$. Specimens shown in *Figures 1a* and *b* were whitened while those in *Figures 1c* and *d* were transparent (referring to *Table 1*). The drawing direction is indicated by the arrow shown in *Figure 1d*. Consistent with the previous findings[16], the fractured surfaces of stress-whitened specimens were more evidently fibrillar and micro-voids formed between the drawn fibres, *Figures 1a* and *b*, while those of the transparent specimens were smoother with a negligible amount of micro-voids, *Figures 1c* and *d*. As the strain rate was increased, the fracture morphologies became more fibrillar and the amount of micro-voids were also increased in the whitened specimens by comparing *Figures 1a* and *b*. The formation of voids in the specimen would have produced strain which would have accounted for some of the imposed strain on the specimen. Consequently, the actual strain in the polymer would be reduced. Although the fractured surface of a transparent specimen could be evidently fibrillar if the drawing rate was high, *Figure 1d*, the integrity of the specimen was high and micro-voiding in this specimen was still negligible when compared with that in the whitened specimens. Because of the limitation of the SEM method, no indication on the crystal perfection, crystal size and the orientation of the crystals could be obtained.

D.s.c.

Figure 2 shows d.s.c. scans of untested iPP specimens (a) without DP fluid and (b) with DP fluid. The presence of the DP fluid had a negligible influence on the d.s.c. scans except for a baseline inclination. This inclination would be expected because the heat capacity would change with the addition of the DP fluid. Since the DP fluid did not give extra endothermic peaks in the testing temperature range, the baseline inclination was adjusted by baseline subtraction during data analysis. No reaction between iPP and DP fluid was observed.

Figure 3 shows the d.s.c. results of untested (a) and drawn (b) to (e) specimens which were immersed in DP

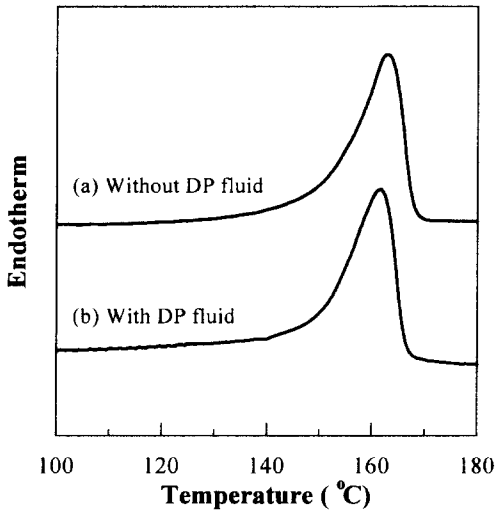

Figure 2 D.s.c. scans of untested iPP specimens showing ignorable influence on the profile of the scan by having the specimen being submerged in a small amount of DP fluid, which was used as a heat conducting medium to ensure an effective and constant thermal contact between the specimen and the testing pan

fluid during analysis. The test conditions of each specimen are indicated in the figure. The shape of the melting endotherm peak of the specimens yielded at 21 and 25°C with a strain rate of $8.33 \times 10^{-1}\ s^{-1}$ was similar to the untested iPP specimen. For these two temperatures, when the strain rate was lowered from 8.33×10^{-1} to 8.33×10^{-2} and $8.33 \times 10^{-3}\ s^{-1}$, the melting peak narrowed and an additional peak began to appear on the low temperature side of the endotherm peak. It can be clearly seen that the additional low melting temperature peak developed further when the yielding temperature increased to 40 and 56°C. At these temperatures, the separation between the two melting peaks appeared larger for specimens tested at a strain rate of $8.33 \times 10^{-1}\ s^{-1}$ than for those at 8.33×10^{-2} and $8.33 \times 10^{-3}\ s^{-1}$. The comparison of *Figure 3* with the whiteness characterization listed in *Table 1* indicates that those specimens which showed two melting peaks were transparent. Furthermore, the two melting peak specimens corresponded to yielding in Region α^{16}, where Process I dominated yielding.

In this d.s.c. analysis, the enthalpy of the iPP specimens was also calculated by measuring the area under the endothermal peak, the background of which was removed by the standard method of single straight line construction available with the instrument. The measurement results of the yielded specimens are shown in *Table 2*. The enthalpy of the untested specimen was about $90\ J\ g^{-1}$ as measured in the same way as the yielded specimens. It can be seen that the value of the enthalpy as measured by d.s.c. for the untested iPP was similar to those of the transparent specimens and observable lower than those of the whitened specimen. Because the value of enthalpy measured from d.s.c. is generally believed to be an indication of the crystallinity of the material, this measure was in contrast to the X-ray results which indicated that a significant reduction in crystallinity occurred for the yielded specimens as shown in the next section. The reason for this contradiction is still not clear.

XRD

In order to investigate the structural changes in the iPP

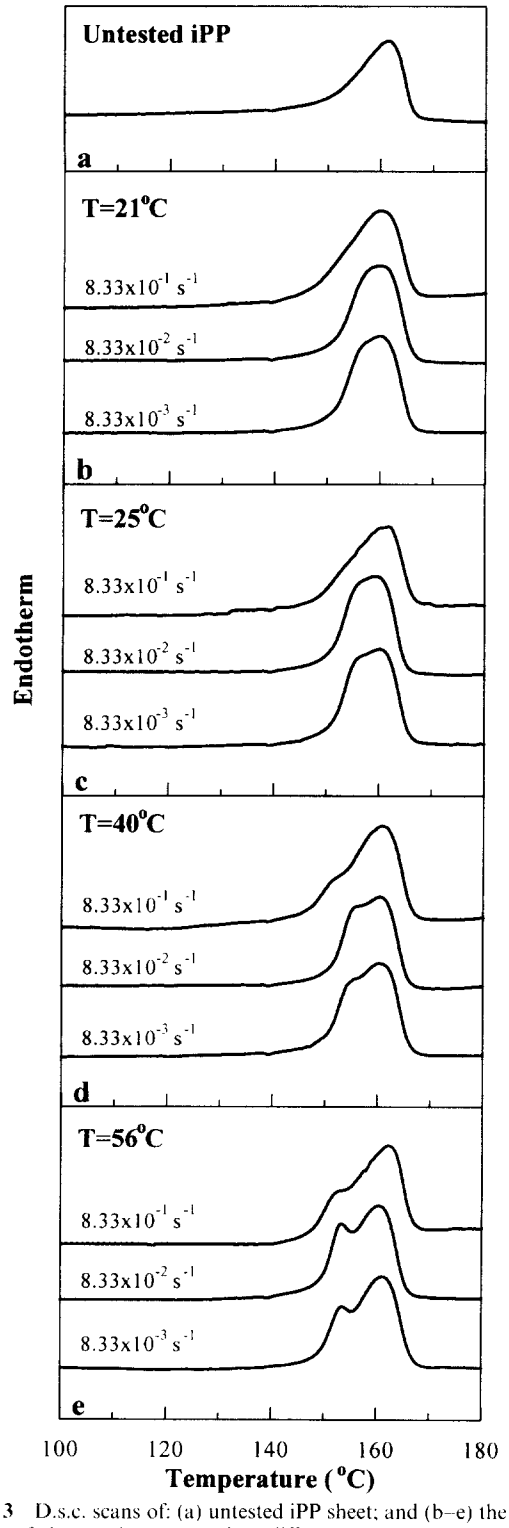

Figure 3 D.s.c. scans of: (a) untested iPP sheet; and (b–e) the necked regions of the specimens tested at different temperatures and strain rates as indicated. The specimens were immersed in DP fluid in d.s.c. analysis

Table 2 The d.s.c. endotherm integration ($J\ g^{-1}$) of iPP specimens tensile tested at different conditions

Temperature	Strain rate (s^{-1})		
(°C)	8.33×10^{-3}	8.33×10^{-2}	8.33×10^{-1}
21	91	90	90
25	96	91	90
40	95	93	99
56	96	95	96

specimens after yielding, the necked regions of representative specimens and also the untested iPP sheet were examined by XRD. *Figure 4* shows a XRD pattern of an untested iPP specimen, which had a typical ringed pattern resulting from the randomly oriented spherulitic structure containing the α-crystals[39]. The first four rings were respectively from the (1 1 0), (0 4 0), (1 3 0), and (0 4 1) reflections of the monoclinic α-crystals[37]. Reflections of (1 1 1) and ($\bar{1}$ 3 1) overlapped with (0 4 1). *Figure 5* shows XRD patterns of specimens yielded respectively under the following conditions: (a) 21°C and $8.33 \times 10^{-3}\ s^{-1}$; (b) 21°C and $8.33 \times 10^{-1}\ s^{-1}$; (c) 56°C and $8.33 \times 10^{-3}\ s^{-1}$; and (d) 56°C and $8.33 \times 10^{-1}\ s^{-1}$. As can be seen, after yielding, the equatorial maxima on the (1 1 0), (0 4 0) and (1 3 0) rings were characteristic of rearrangement of the crystallites in which the monoclinic crystallites were re-oriented with their c-axis nearly parallel to the drawing direction and the b-axis perpendicular to the drawing direction. The fibrillar structure, that formed after the iPP specimens were drawn, was also aligned with the drawing direction. Although the additional d.s.c. peak from the transparent specimens may have suggested the presence of a new crystal structure formed during drawing, no new crystalline phase could be found from this XRD investigation.

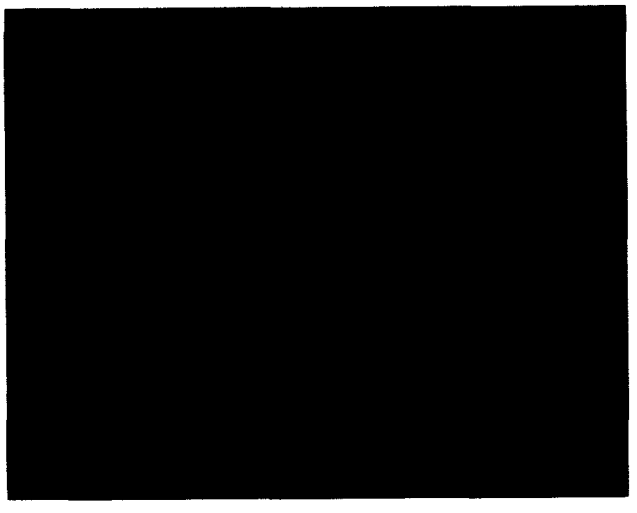

Figure 4 XRD pattern taken from an untested iPP sheet

At the low strain rate of $8.33 \times 10^{-3}\ s^{-1}$, there was still a proportion of drawn iPP that remained poorly oriented for the specimen drawn at 21°C (*Figure 5a*). This was indicated by the long diffraction arcs which could still be seen in the XRD pattern. In contrast, almost all of the

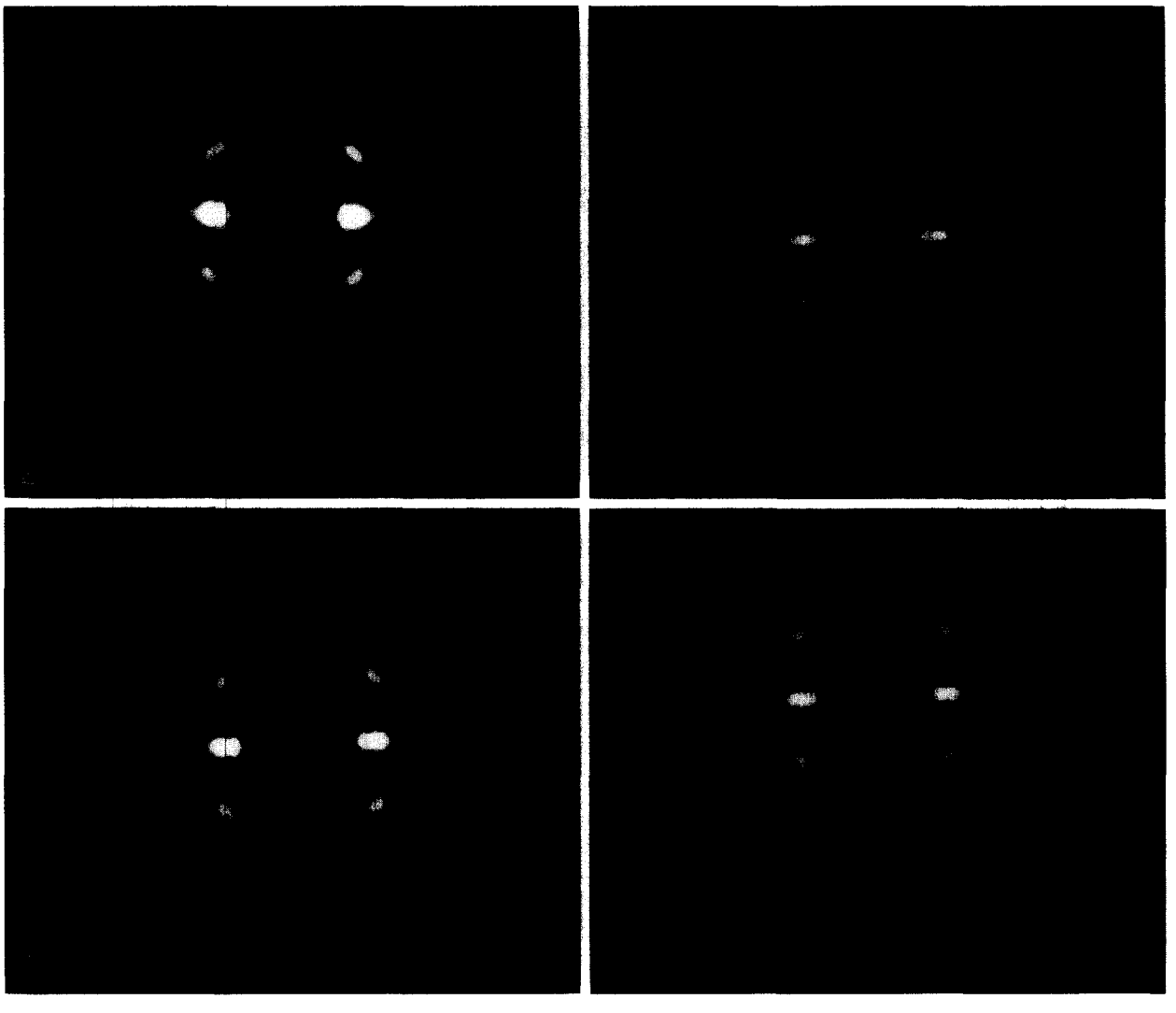

Figure 5 XRD patterns of the necked regions of specimens tested respectively at: (a) 21°C and $8.33 \times 10^{-3}\ s^{-1}$; (b) 21°C and $8.33 \times 10^{-1}\ s^{-1}$; (c) 56°C and $8.33 \times 10^{-3}\ s^{-1}$; and (d) 56°C and $8.33 \times 10^{-1}\ s^{-1}$

crystallites were oriented when the specimens were drawn at $8.33 \times 10^{-1}\,s^{-1}$ and 56°C (*Figures 5b–d*). It seemed that an increase in both the strain rate and temperature increased the directionality of the crystallites. Drawing at a high rate would create a high local stress to align the crystallites with the drawing direction while an increase in temperature would increase the chain mobility, and enhance reorientation of the crystallites. Both factors would enhance the directionality of the drawn specimens.

Apart from the directionality of the monoclinic crystallites, the size of the crystallites seemed to vary with the drawing conditions as indicated by the degree of overlapping between the equatorial reflections, i.e. the reflections of (1 1 0), (0 4 0) and (1 3 0). Clearly, these reflections were more diffuse and thus overlapped more for the specimen yielded at $8.33 \times 10^{-3}\,s^{-1}$ and 21°C, *Figure 5a*, than for the rest of the specimens shown in the same figure. However, the difference between the rest of the specimens in terms of the degree of overlapping could not be seen clearly by visual examination of the diffraction patterns.

Given the crystal structure of a compound, its XRD pattern may be calculated. Using the theoretical intensities for a structure, an observed diffraction pattern may be simulated by applying theoretical peak shape functions to the intensities. Furthermore, the observed and calculated patterns may be matched through refinement of the crystal structures or diffraction peak models in procedures such as minimization of least-squares-differences. This technique of profile-fitting of XRD patterns is known as the Rietveld technique, after its innovator[40], and provides a method of extracting crystallographic and microstructural information from a diffraction pattern. The uniform and non-uniform crystallite strain may be obtained from unit cell dimensions and Gaussian diffraction peak widths,

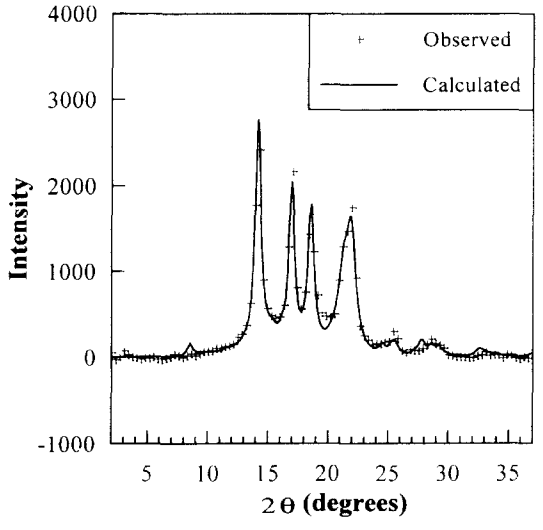

Figure 6 Observed (symbol +) and calculated (solid line) XRD trace of an untested iPP specimen

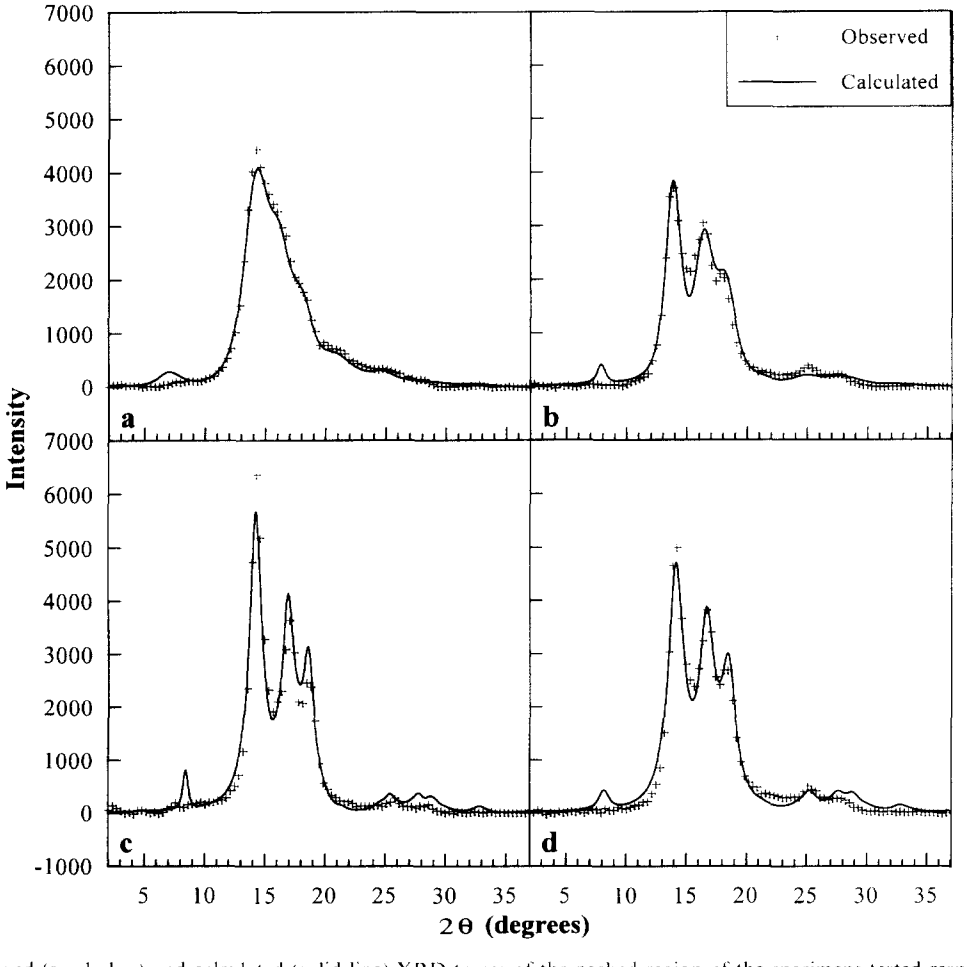

Figure 7 Observed (symbol +) and calculated (solid line) XRD traces of the necked region of the specimens tested respectively at: (a) 21 C and $8.33 \times 10^{-3}\,s^{-1}$; (b) 21 C and $8.33 \times 10^{-1}\,s^{-1}$; (c) 56 C and $8.33 \times 10^{-3}\,s^{-1}$; and (d) 56 C and $8.33 \times 10^{-1}\,s^{-1}$

Table 3 Microstructural parameters obtained from the Rietveld refinement of iPP XRD patterns

Specimen	X (%)	P_x	P_a	d_x (Å)	d_a (Å)	a (Å)	b (Å)	c (Å)
Untested	80	1.000[a]	1.000	288	78	6.66	21.92	6.57
A	11	4.401[b]	1.232	50	24	6.20	20.88	6.50
B	10	1.919[c]	1.389	26	31	6.50	20.88	6.50
C	26	1.330	1.204	131	23	6.60	20.96	6.50
D	20	1.461	0.852	93	21	6.50	20.86	6.50

The specimens *A* to *D* were tested respectively at the following temperatures and strain rates: 21°C, $8.33 \times 10^{-3}\ s^{-1}$; 21°C, $8.33 \times 10^{-1}\ s^{-1}$; 56°C, $8.33 \times 10^{-3}\ s^{-1}$; and 56°C, $8.33 \times 10^{-1}\ s^{-1}$

[a,b,c] Crystalline with respectively 36%, 6% and 3% [1 $\bar{1}$ 1] preferred orientation

X = crystallinity

P_x, P_a = [0 0 1] preferred orientation parameter of crystalline and amorphous phase, respectively

d_x, d_a = scattering element size of crystalline and amorphous, respectively

a, b, c = a-axis, b-axis and c-axis unit cell dimensions, respectively

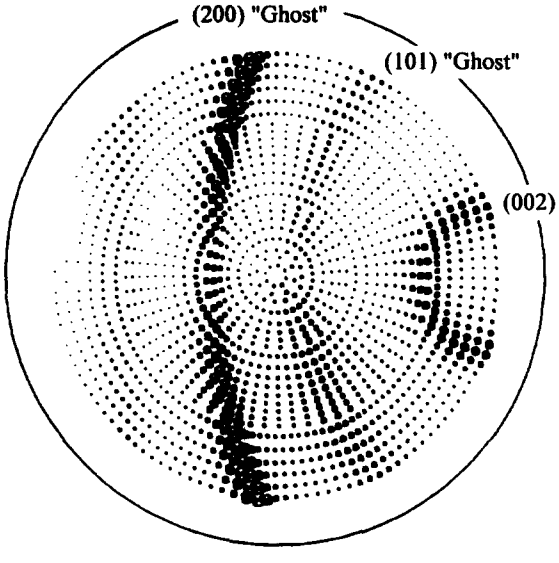

Figure 8 X-ray (0 0 2) pole figure of iPP drawn at 21° and $8.33 \times 10^{-1}\ s^{-1}$ (note that (2 0 0) and (1 0 1) 'ghost' can also be seen)

respectively. Crystallite sizes are related to the Lorentzian peak widths through the Scherrer formula[41]. The preferred orientation of the crystallites may be measured by using the March equation[42].

In the present analysis, the size of each type of scattering element, i.e. the coherent scattering domain, was determined using the Scherrer equation with the Gaussian peak width deconvoluted from the instrumental broadening component of the diffraction profile[41]. Weight fractions of crystalline and amorphous material were found from the Rietveld scale factors[43]. The crystallites or the chain orientation are indicated by the March function preferred orientation parameter[42]. *Figure 6* presents the observed XRD trace (symbol +) and the corresponding fitted profile from the Rietveld analysis (solid line) of an untested specimen, whereas *Figure 7* shows those of the yielded specimens which were respectively yielded at: (a) 21°C and $8.33 \times 10^{-3}\ s^{-1}$; (b) 21°C and $8.33 \times 10^{-1}\ s^{-1}$; (c) 56°C and $8.33 \times 10^{-3}\ s^{-1}$; and (d) 56°C and $8.33 \times 10^{-1}\ s^{-1}$.

As can be seen in *Table 3*. The observed XRD traces shown in *Figures 6* and *7* for the untested and the equatorial profiles of the yielded specimens agreed well with the XRD diffraction patterns shown in *Figures 4* and *5*, and the Rietveld analysis gave satisfactory curve fittings to the observed traces. Important structural parameters obtained from the Rietveld analysis are shown in *Table 3*.

The crystallinities (X) of the yielded specimens, typically $X \sim 10$–30%, were much lower than that of the untested specimen, $X \sim 80\%$. Furthermore, the whitened (*A* and *B*) specimens had even lower crystallinities than the transparent ones (*C* and *D*). There was also a significant reduction in scattering element sizes (d_x for crystalline phase and d_a for amorphous phase) after yielding and the scattering element size for the crystalline phase of the whitened specimens (*A* and *B*) was even smaller than the transparent ones (*C* and *D*). The above observation indicates that, during the yielding process, the crystalline lamellae were not just broken up into small crystal blocks but also that a considerable portion of them were transformed into an amorphous phase with the reduction in crystallinity being greater and resultant crystal size being smaller in the whitened specimens.

In a previous study[41], the Rietveld technique was applied in the analysis of cast PHB for measurement of microstructural parameters. In the case of drawn polymers, texture may make such analyses difficult. However, in the present study of drawn iPP, preferred orientation rather than texture is evident. According to the pole figure measured for the (0 0 2) reflection of iPP as shown in *Figure 8*, the distribution of this plane is over the entire 160° arc sampled. A 'ghost' of the (2 0 0) reflections is also evident over the same angular range, about 70° from the former pole. The approximate 70° angle is the appropriate crystallographic relationship between the (0 0 2) and (2 0 0) of iPP. Therefore, the pole figure indicates an alignment of the {0 0 l} planes perpendicular to the drawing direction, and random distribution of the other principle zones about this axis, i.e. preferred orientation in [0 0 1].

A microstructural model could be constructed with isolated sets of {hk0} and {0 0 l} intensities aligned perpendicular to and parallel to the drawing direction, respectively, but randomly oriented around [0 0 1]. Therefore, Rietveld analysis could be applied to the equatorial scans of drawn iPP in this study, using the appropriately chosen preferred orientation corrections.

Rietveld analyses reveal the crystalline fractions of iPP drawn at 21°C to be more heavily oriented than those drawn at 56°C, i.e. P_x is larger for specimens *A* and *B*, than for specimens *C* and *D*. This finding may be a result of some crystallite shape effect, in agreement with the SEM study (*Figure 1*) which shows the low temperature tensile specimens to be more fibrillar, although an SAXS study is necessary for confirmation of these WAXS results.

The Rietveld analysis also revealed that 36% of the crystallites in the untested specimen were of [1 $\bar{1}$ 1] preferred orientation (*Table 3*). This probably resulted from the preparation of the iPP thin sheet during which spherulites were preferably nucleated from the surfaces of the sheet. It is interesting to note in *Table 3* that in the whitened specimens there was still a certain amount of crystallites preferably oriented along the [1 $\bar{1}$ 1]. It was 6% in the specimen drawn at 21°C and $8.33 \times 10^{-3}\ s^{-1}$ and 3% in the one drawn at 21°C and $8.33 \times 10^{-1}\ s^{-1}$. In the transparent specimens, the [1 $\bar{1}$ 1] preferred orientation was not detectable.

The Rietveld analysis indicated that the orientation of crystallites (P_x) in the transparent specimens was more

thoroughly in the [0 0 1] alignment after yielding than in the whitened specimens and moreover that the resultant crystallite size was finer in the whitened specimens. The yielding conditions for the transparent specimens of high temperature and low strain rate would allow greater intermolecular movement to occur. This would reduce the local stress on the crystal blocks and results in the crystal block having a reduced friction against rotation to its favourable orientation in the fibril without being broken further.

This was consistent with the measured orientation in the amorphous regions. After yielding, [0 0 1] preferred orientation of the molecular chains in the amorphous phase (P_a) of the specimen was stronger in the whitened specimens than in the transparent ones. The higher strain rate and lower temperature of the whitened specimens would reduce inter-molecular movement making it difficult for the chains to relax resulting in higher local stresses and greater orientation of the amorphous regions in these specimens.

The scattering elements in the yielded specimens were deformed as indicated by the reduction of the refined unit cell parameters, a and b, from the initial crystal structure shown in *Table 3*. This reduction is consistent with the result of stretching along the [0 0 1] direction and can be seen as an indication of the presence of residual stress in the drawn specimen. However, the difference in the unit cell distortion between the whitened and transparent specimens could not be established in the present study. Differences may have been seen if the XRD traces were collected as the specimens were yielding. This would minimize the influence of stress relaxation after the specimens were unloaded.

The origin of the two d.s.c. endothermal peaks of the transparent iPP

The search of the physical origin of the additional d.s.c. melting peak of the transparent iPP specimens has not reached a conclusive result in this study in spite of the progress made in the microstructural characterization of the yielded specimens (see above) by XRD investigation, particularly the Rietveld analysis. The current understanding and knowledge on this additional d.s.c. peak is as follows.

(i) *No new crystalline phase.* In the XRD investigation, no new crystalline phase was found in any of the XRD patterns from the transparent specimens with the present instrument and diffraction conditions. This result suggested that the additional d.s.c. melting peak in the transparent specimens was not due to the formation of any new crystalline phase.

(ii) *The crystallinity as determined by XRD and d.s.c.* The crystallinity of yielded iPP specimens as determined from Rietveld analysis showed a significant reduction as compared with the untested specimens, e.g. from 80% to about 25% for the transparent specimens and a further reduction to about 10% for the whitened specimens (*Table 3*). However, the enthalpy differences of these iPP specimens as determined by d.s.c. were insignificant. Typically 10–11% crystallinity is found for iPP drawn at 21°C (*Table 3*), with 90–91 J g^{-1} for the melting endotherm (*Table 2*), whereas 20–26% crystallinity is found for the iPP drawn at 56°C (*Table 3*), with 95–96 J g^{-1} for its melting (*Table 2*). One consideration for this apparent inconsistency between XRD and d.s.c. on crystallinity is that the d.s.c. endothermal peaks from this material may not be necessarily from crystalline phases. A further study along this line of thought would be on the formation of any smectic phases during yielding and the role of such phases in determining the profile of d.s.c. scan. Another consideration is that significant recrystallization may have occurred during the heating process of d.s.c. analysis. If this is true, a further question is raised as to what microstructure causes this recrystallization to give rise to two melting peaks only for the transparent but not for the whitened specimens. The answer to this further question is still unknown.

(iii) *Crystal size.* It is known that, for nano-crystals, their melt temperature decreases with a decrease in crystal size. This effect has been considered to be the physical origin for multiple melting point behaviour of iPP induced by annealing treatment[44]. However, the average crystal size of the yielded specimens found by XRD was inconsistent with the above consideration if any possible recrystallization during d.s.c. scanning is ignored. This is because the transparent specimens had a larger average crystal size than that of the whitened specimens (*Table 3*) and thus the expected shift of melting peak towards lower temperatures due to crystal size should be less than that of the whitened specimens. However, correlating with the ratio of sizes of crystalline and amorphous scattering elements from Rietveld analyses, the greater is the d_x/d_a ratio of *Table 3*, the more distinct are the two peaks of the corresponding d.s.c. trace.

(iv) *Chain ordering.* Although the endotherm integrations yield similar values independent of the yielding history of the specimens (*Table 2*), the appearance of the endotherm alters significantly between treatments as shown in *Figure 3* that might correspond to chain ordering. Chain ordering divides the α crystallites of iPP into two types: α_2, the ordered limiting structure, which has a symmetry of $P2_1/c$[52] with a well-defined disposition of 'up' and 'down' helices in the unit cell[37,53]; and α_1, the disordered limiting structure, which has a symmetry of $C2/c$[52] with a random distribution of 'up' and 'down' chains in each site of the unit cell[39]. This chain ordering is another factor that can alter the d.s.c. profile. It has been found in X-ray investigations[44–50] that various factors, including annealing treatment, high temperature conditioning, d.s.c. scanning rate, tensile draw rate, can affect the ordering of the α-crystallites by changing 'up' and 'down' positioning of the chains in the crystallites while the unit cell remained substantially unchanged. The variation in chain ordering in the α-crystallites has been suggested to be a microscopic origin for the double d.s.c. peaks of α-iPP[46–48,51]. However it has not been possible in this work to determine proportions of α_1 and α_2 crystallites in the specimens. Further work on this topic would be worthwhile.

CONCLUSIONS

It was found by SEM that the whitening of the necked region of tensile yielded iPP specimens was associated with the presence of a large amount of micro-voids and a highly fibrillar morphology. In transparent specimens, the fracture surface was smooth and micro-voids were rarely observed.

A d.s.c. technique for studying tensile yielded iPP specimens was developed in the work. In this technique, the specimen of drawn iPP was immersed in a drop of diffusion pump fluid in the d.s.c. testing pan in the d.s.c. analysis in order to overcome the influence of the thermal contraction of the specimens upon melting on the accuracy of the measurement. With this technique, reproducible and satisfactory d.s.c. results were obtained. By using this improved d.s.c. technique, two melting peaks were found in the necked regions of the transparent specimens which were yielded typically at high temperatures and low strain rates. There was only one endotherm peak found in the whitened specimens, the typical yielding conditions of which were low temperatures and high strain rates.

XRD investigations showed that there was no new crystal structure formed in the drawn iPP specimens, although an additional lower d.s.c. melting peak was observed with the transparent specimens. The Rietveld analysis on the equatorial XRD traces showed that the α-crystals in the whitened specimens were broken into finer pieces than in the transparent specimens. The analysis also showed that the chains in amorphous regions and crystallites were aligned more thoroughly along the loading direction in the whitened specimens than in the transparent ones.

REFERENCES

1. Peterlin, A. and Baltá-Calleja, F. J., *J. Appl. Phys.*, 1969, **40**, 4238.
2. Ward, I. M., *Mechanical Properties of Solid Polymers*, 2nd edn. John Wiley and Sons, 1983.
3. Kammer, H. W., Kummerloewe, C., Greco, R., Mancarella, C. and Martuscelli, E., *Polymer*, 1988, **29**, 963.
4. Osawa, S. and Porter, R. S., *Polymer*, 1994, **35**, 540.
5. Lazurkin, Y. S., *J. Polym. Sci.*, 1958, **30**, 595.
6. Robertson, R. E., *J. Chem. Phys.*, 1966, **44**, 3950.
7. Marshall, I. and Thompson, A. B., *Proc. Roy. Soc. A*, 1954, **221**, 541.
8. Argon, A. S., Andrews, R. D., Godrick, J. A. and Whitney, W., *J. Appl. Phys.*, 1968, **39**, 1899.
9. Brown, N., *Mater. Sci. Eng.*, 1971, **8**, 69.
10. Bochum, A. S., *Kunststoffe*, 1982, **72**, 791.
11. Peterlin, A., *J. Polym. Sci*, 1965, **C9**, 61.
12. Young, R. A. and Sokthivel, A., *J. Appl. Cryst.*, 1988, **21**, 416.
13. Lutz, C., Fishcher, G. and Eyerer, P., *ANTEC'87*, 1018, 1987.
14. Friedrich, K. in *Advances in Polymer Science*, ed. H. H. Kausch, Vol. 52/53. Springer-Verlag, Berlin, 1983 p. 225.
15. Kramer, E. J. and Berger, L. L., *ibid.*, Vol. 91/92, 1990, p. 1.
16. Liu, Y. and Truss, R. W., *J. Polym. Sci. Polym. Phys. Ed.*, 1994, **32**, 2037.
17. Yan, R. and Jiang, B., *J. Polym. Sci. Polym. Phys. Ed.*, 1993, **31**, 1089.
18. Turetskii, A. A., Chvalun, S. N., Baranov, A. O., Zubov, Yu. A. and Prut, E. V., *Vysokomol. Soyed. Ser. A*, 1988, **30**, 1878.
19. Liu, Y. and Truss, R. W., *Proceedings of the 3rd Pacific Polymer Conference*, 1993, p. 413.
20. Tobolsky, A. V. and Andrews, R. D., *J. Chem. Phys.*, 1945, **13**, 3.
21. Argon, A. S., *Phil. Mag.*, 1973, **28**, 839.
22. Bowden, P. B. and Raha, S., *Phil. Mag.*, 1974, **29**, 149.
23. Tate, K. R., Perrin, A. R. and Woodhans, R. T., *Polym. Eng. Sci.*, 1988, **28**, 740.
24. Eyring, H., *J. Chem. Phys.*, 1936, **4**, 283.
25. Glasstone, S., Laidler, K. J. and Eyring, H., *The Theory of Rate Processes*. McGraw-Hill, 1941, pp. 480–483.
26. Ree, T. and Eyring, H., *J. Appl. Phys.*, 1955, **26**, 793.
27. Robertson, R. E., *J. Appl. Polym. Sci.*, 1963, **7**, 443.
28. Roetling, J. A., *Polymer*, 1965, **6**, 311.
29. Roetling, J. A., *Polymer*, 1965, **6**, 615.
30. Roetling, J. A., *Polymer*, 1966, **7**, 303.
31. Bauwens-Crowet, C., Bauewns, J. C. and Homes, G., *J. Polym. Sci. A-2*, 1969, **7**, 735.
32. Yoon, H. N., Pae, K. D. and Sauer, J. A., *J. Polym. Sci. Polym. Phys. Ed.*, 1976, **14**, 1611.
33. Truss, R. W., Clarke, P. L. Duckett, R. A. and Ward, I. M., *J. Polym. Sci. Polym. Phys. Ed*, 1984, **22**, 191.
34. Capaccio, G., Crompton, T. A. and Ward, I. M., *J. Polym. Sci. Polym. Phys. Ed.*, 1976, **14**, 1641.
35. Pals, D. T. F., Van Der Zee, P. and Albers, J. H. M., *J. Macromol. Sci.–Phys.*, 1972, **B6**, 739.
36. Taylor, J. C., *Powder Diffraction*, 1991, **6**, 2.
37. Mencik, Z., *J. Macromol. Sci.–Phys.*, 1972, **B6**, 101.
38. Peterlin, A., *J. Mater. Sci.*, 1971, **6**, 490.
39. Natta, G. and Corradini, P., *Nuovo Cimento Suppl.*, 1960, **15**, 40.
40. Rietveld, H. M., *Acta Cryst.*, 1967, **22**, 151.
41. Langford, J. I., Louer, D., Sonneveld, E. J. and Visser, J. W., *Powder Diffraction*, 1986, **1**, 211.
42. Dollase, W. A., *J. Appl. Cryst.*, 1986, **19**, 267.
43. Calos, N. J. and Kennard, C. H. L., *Polymer*, 1994, **35**, 4595.
44. Pae, K. D. and Sauer, J. A., *J. Appl. Polym. Sci.*, 1968, **12**, 1901.
45. Hikosaka, M. and Seto, R., *Polymer J.*, 1973, **5**, 111.
46. Corradini, P., Napolitano, R., Oliva, L., Petraccone, V., Pirozzi, B. and Guerra, G., *Makromol. Chem., Rapid Commun.*, 1982, **3**, 753.
47. Guerra, G., Petraccone, V., Corrandini, P., De Rosa, C., Napolitano, R. and Pirozzi, B., *J. Polym. Sci., Polym. Phys. Ed.*, 1984, **22**, 1029.
48. De Rosa, C., Guerra, G., Napolitano, R., Petraccone, V. and Pirozzi, B., *Eur. Polym. J.*, 1984, **20**, 937.
49. Nichols, M. E. and Robertson, R. E., *J. Polym. Sci., Polym. Phys. Ed.*, 1992, **30**, 305.
50. Fillon, B., Wittmann, J. C., Lotz, B. and Thierry, A., *J. Polym. Sci., Polym. Phys. Ed.*, 1993, **31**, 1383.
51. Yadav, Y. S. and Jain, P. C., *Polymer*, 1986, **27**, 721.
52. *International Tables for X-Ray Crystallography*, Vol. I. Kynoch, Birmingham, 1952.
53. Hikosaka, M. and Seto, T., *Polymer J.*, 1973, **5**, 111.